Available online at www.sciencedirect.com
SCIENCE DIRECT
Journal of Molecular Catalysis A: Chemical 252 (2006) 120–124
JOURNAL OF MOLECULAR CATALYSIS A: CHEMICAL
www.elsevier.com/locate/molcata

A sonochemical route to visible-light-driven high-activity $BiVO_4$ photocatalyst

Lin Zhou, Wenzhong Wang *, Shengwei Liu, Lisha Zhang, Haolan Xu, Wei Zhu

State Key Laboratory of High Performance Ceramics and Superfine Microstructure, Shanghai Institute of Ceramics, Chinese Academy of Sciences, 1295 DingXi Road, Shanghai 200050, PR China

Received 5 January 2006; accepted 24 January 2006
Available online 24 March 2006

Abstract

Visible-light-induced $BiVO_4$ photocatalyst with monoclinic scheelite structure has been successfully synthesized via a facile sonochemical method. The as-prepared $BiVO_4$ photocatalyst exhibited relatively high surface areas, consisting of primary nanocrystals with average size of ca. 50 nm. The $BiVO_4$ nanocrystals showed a strong absorption in the visible light region and the band gap was estimated to be ca. 2.45 eV, representing an obvious blue-shift compared with that of the bulk sample. The photocatalytic activities were also evaluated by decolorization of methyl orange under visible light ($\lambda > 400$ nm). The results indicate that the photodegradation rate of as-prepared $BiVO_4$ nanocrystals is quite high, up to 90% in 30 min, which is much better than that of the reference sample prepared by solid-state reaction (ca. 8%) and the standard photocatalyst P25 (ca. 6%) under the same conditions.

Keywords: $BiVO_4$ nanocrystals; Photocatalysis; Sonochemical synthesis; Visible light; Photodegradation

1. Introduction

Recently, the decomposition of harmful organic and inorganic pollutants using photosensitized semiconductors as catalyst has attracted increasing attention [1,2]. Particularly, TiO_2 has been well known as an effective photocatalyst and its photocatalytic behavior has been extensively studied [3–6]. However, TiO_2 only respond to UV light which occupies only 4% of the whole solar energy, while the visible light accounting for 43% is open to exploiture. The development of visible-light-driven photocatalysts, therefore, has become one of the most challenging topics recently.

Bismuth vanadate ($BiVO_4$) has been recently recognized as a strong photocatalyst for water splitting and pollutant decomposing under visible light irradiation [7–9]. $BiVO_4$ exists in three phases, monoclinic sheelite, tetragonal zircon and tetragonal sheelite [10]. The photocatalytic properties of $BiVO_4$ are strongly related to its crystal phase, for example, the photocatalytic activity of monoclinic phase was much higher than that of the other two [11]. Several methods have been reported for the preparation of $BiVO_4$, such as solid-state reaction, co-precipitation, hydrothermal treatment and metalorganic decomposition [12–15]. However, most of these methods require high reaction temperature, or long reaction time, and the particle size of products is generally rather big. On the other hand, sonochemical techniques have been recently developed for the fast synthesis of nanosized functional inorganic materials [16–19]. The unique chemical effects of ultrasound arise from acoustic cavitation, that is, the ultrasonic vibrations produce microscopic bubbles (cavities), which expand and implode violently, creating millions of shock waves. During the collapse of the bubble, very high temperatures (>5000 K), pressures (>20 MPa) and cooling rates (>10^{10} K/s) can be achieved [20]. It is expected that sonochemical approach may create inorganic materials with smaller crystal size and higher surface area, which is recognized to be beneficial to the photocatalytic activities [19]. However, to the best of our knowledge, the sonochemical approach for $BiVO_4$ photocatalyst has not yet been reported.

In this study, we report a facile sonochemical route for the synthesis of visible-light-driven $BiVO_4$ photocatalyst with high efficiency. The composition and microstructure of as-prepared

* Corresponding author. Tel.: +86 21 5241 5295; fax: +86 21 5241 3122.
E-mail address: wzwang@mail.sic.ac.cn (W. Wang).

1381-1169/$ – see front matter © 2006 Elsevier B.V. All rights reserved.
doi:10.1016/j.molcata.2006.01.052

products were investigated. The photocatalytic activity was also evaluated, in comparison with that of reference samples prepared by the solid-state reaction and that of standard photocatalyst P25.

2. Experimental

2.1. Synthesis

All the reagents used in our experiments were of analytical purity and were used as received from Shanghai Chemical Company. In a typical preparation, aqueous solutions of $Bi(NO_3)_3{\cdot}5H_2O$ and NH_4VO_3 were mixed together in 1:1 molar ratio, the mixture was then stirred for 1 h at room temperature. Afterward, the mixture was exposed to high-intensity ultrasound irradiation for 60 min. The yellow precipitates were centrifuged, washed with de-ionized water and absolute ethanol, and then dried at 353 K in air for 10 h. For comparison, bulk $BiVO_4$ was also prepared by solid-state reaction according to Ref. [14].

2.2. Characterization

The powder X-ray diffraction (XRD) patterns of the as-synthesized samples were measured on a D/MAX 2250 V diffractometer (Rigaku, Japan) using monochromatized Cu Kα ($\lambda = 0.15418$ nm) radiation at a scanning rate of $4^\circ\ min^{-1}$ with the 2θ ranging from 10° to 70°. The accelerating voltage and applied current were 40 kV and 100 mA, respectively. The morphologies and microstructures of as-prepared samples were examined with transmission electron microscopy (TEM, JEOL JEM-2100F; accelerating voltage: 200 kV) and scanning electron microscopy (SEM, JSM-6700F). The compositions were analyzed using an X-ray energy dispersive spectrometer (EDS) equipped with the TEM. Optical absorbance spectra of the samples were obtained on an UV–vis spectrophotometer (Shimadzu UV-3101). Nitrogen adsorption–desorption measurements were conducted at 77.35 K on a Micromeritics Tristar 3000 analyzer after samples were degassed at 200 °C for 6 h. The Brunauer–Emmett–Teller (BET) surface area was estimated using adsorption data in a relative pressure range from 0.05 to 0.3.

2.3. Photocatalytic test

Photocatalytic activities of the $BiVO_4$ samples were evaluated by photocatalytic decolorization of methyl orange under visible light. A 500 W high-pressure Hg lamp was used as a light source with a 400 nm cutoff filter to provide visible light irradiation. Experiments were performed at ambient temperature as follows: same amount (0.6 mmol) of photocatalyst $BiVO_4$ or TiO_2 was added into 60 mL of 40 mg/L methyl orange (MO) solution. Before illumination, the solution was stirred for 30 min in the dark in order to reach the adsorption–desorption equilibrium for MO and dissolved oxygen. The concentrations of the MO were monitored using a UV-2003 UV–vis spectrophotometer by checking the absorbance at 464 nm during the photodegradation process.

3. Results and discussion

3.1. Formation of the $BiVO_4$ crystals

The composition and phase transformation process of $BiVO_4$ products according to the ultrasonic reaction time was investigated using XRD measurement. The XRD patterns of $BiVO_4$ samples obtained after ultrasonic irradiation for 30 and 60 min are shown in Fig. 1(a and b), respectively. When ultrasonic irradiation time was 30 min, as shown in Fig. 1(a), the diffraction pattern indexed to monoclinic $BiVO_4$ (JCPDS No.: 14-0688) was detected, along with tetragonal $BiVO_4$ (JCPDS No.: 14-0133). The percentage of monoclinic phase has been calculated based on the normalized ratios of relative intensities for (1 2 1) peak of monoclinic $BiVO_4$ to that for (2 0 0) peak of tetragonal $BiVO_4$ [13], i.e.:

$$V_{\text{mono}} = \frac{I_{\text{mono}(1\,2\,1)}}{I_{\text{mono}(1\,2\,1)} + I_{\text{tetra}(2\,0\,0)}}$$

V_{mono}, $I_{\text{mono}(1\,2\,1)}$ and $I_{\text{tetra}(2\,0\,0)}$ denote the percentage of monoclinic phase, the relative intensity of (1 2 1) peak for monoclinic phase and that of (2 0 0) peak for tetragonal phase, respectively. The calculated volume fraction of monoclinic phase is only 47%. As the ultrasonic time increased, the peaks for tetragonal $BiVO_4$ gradually disappeared, and the peaks for monoclinic $BiVO_4$ became dominant. In 60 min, all the diffraction peaks (Fig. 1(b)) were indexed to be a pure monoclinic phase of $BiVO_4$. At the corner of Fig. 1, the part of XRD pattern near 19° is widened to show the characteristic split of the monoclinic scheelite phase. Thus, it was supposed that a phase transformation from tetragonal to monoclinic phase of $BiVO_4$ had taken place during the ultrasonic irradiation. This result demonstrated that pure monoclinic $BiVO_4$, which was reported to be of higher photocatalytic activity, could be synthesized by ultrasonic irradiation for short time. For comparison, the XRD pattern for samples obtained by solid-state reaction (SSR) is also showed in Fig. 1(c). It revealed

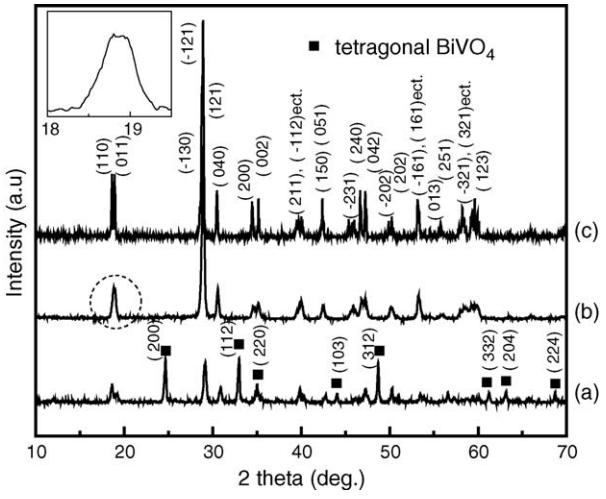

Fig. 1. XRD patterns of $BiVO_4$ crystals prepared by ultrasonic irradiation for 30 min (a), 60 min (b) and by solid-state reaction (c). Inset: the widened part of XRD pattern near 19°, showing the characteristic split of the monoclinic scheelite phase.

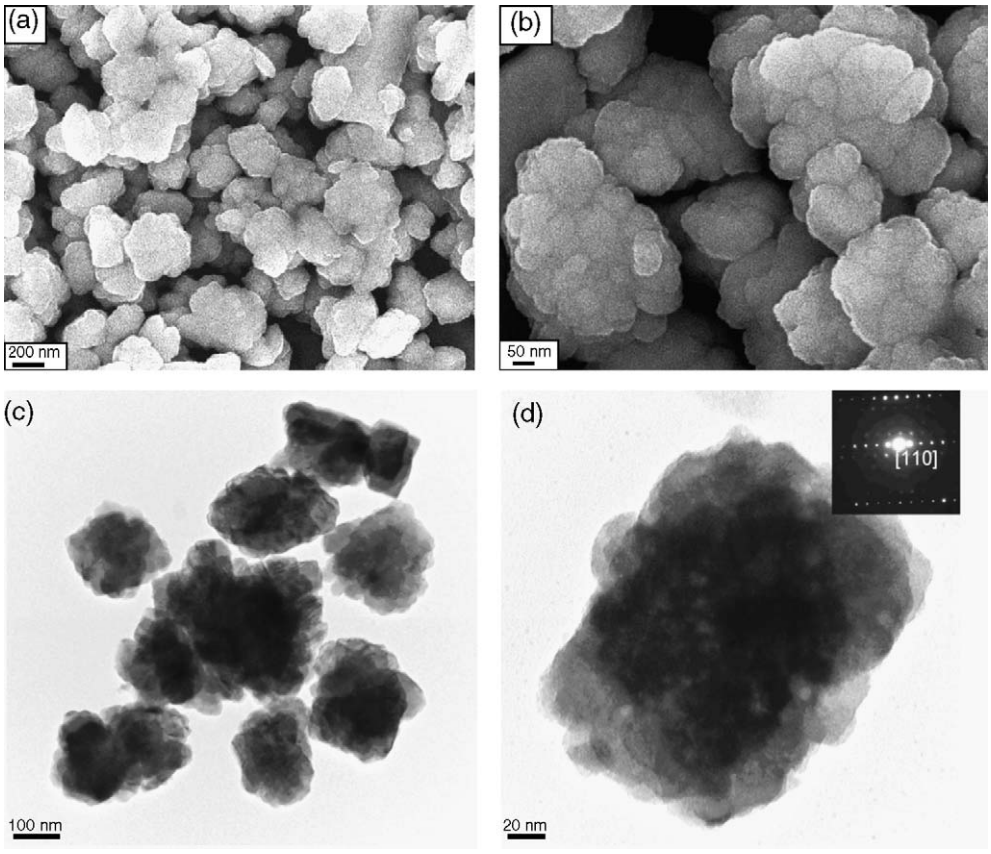

Fig. 2. SEM (a and b), TEM (c and d) images and SAED (inset in d) pattern of UR-$BiVO_4$ samples.

that a pure monoclinic phase could also be obtained by SSR method. The average crystal size of pure monoclinic $BiVO_4$ prepared by ultrasonic irradiation (UR-$BiVO_4$) was estimated to be about 41 nm based on Scherrer equation, which was much smaller than that (ca. 186 nm) of monoclinic $BiVO_4$ prepared by SSR method (SSR-$BiVO_4$).

3.2. Microstructures of the UR-$BiVO_4$ crystals

The morphology and microstructure of the UR-$BiVO_4$ particles were revealed by scanning electron microscopy (SEM) and transmission electron microscopy (TEM). Fig. 2(a and b) are the SEM images of the UR-$BiVO_4$ samples, showing that they are composed of particles with the size ranging from 100 to 300 nm. Close observation indicates these $BiVO_4$ particles are composed of even smaller primary nanocrystals with crystalline size of about several tens nanometers. This fine structure was further demonstrated by the corresponding TEM images of the primary particles. Fig. 2(c) shows that the UR-$BiVO_4$ particles are generally ca. 200 nm in size. And it is clearly seen that these UR-$BiVO_4$ particles are composed of many primary crystals, which are confirmed to be ca. 50 nm by a higher magnification TEM image for an individual UR-$BiVO_4$ particle (Fig. 2(d)). The crystalline size is in good agreement with that evaluated using Scherrer equation based on XRD patterns. The composition is analyzed by EDS and the result is in well accordance with that of XRD patterns. On the other hand, to our surprise, the corresponding selected area electron diffraction (SAED) pattern (Fig. 2(d), inset) of an individual UR-$BiVO_4$ particle exhibited a monocrystalline-like diffraction pattern, indicating that the primary nanocrystals that constructed the entire UR-$BiVO_4$ particle shared the same orientation direction along [1 1 0] direction. In addition, the Brunauer–Emmett–Teller (BET) surface area of UR-$BiVO_4$ samples was also estimated using N_2 adsorption data. The BET surface area of UR-$BiVO_4$ samples was estimated to be ca. 4.16 m^2/g, which was much higher than of the reference SSR-$BiVO_4$ sample of ca. 0.26 m^2/g.

3.3. Band gap of the UR-$BiVO_4$ nanocrystals

It is well known that the electronic structure of the semiconductor usually plays a crucial role in its photocatalytic activity [21,22]. Recently, the electronic structure of $BiVO_4$ has been reported [23] based on the DFT calculations. It is pointed out that the valence band (VB) of $BiVO_4$ is composed of hybridized Bi 6s and O 2p orbitals, whereas the conduction band is composed of V 3d orbitals. The charge transfer upon photo-excitation is thus supposed to occur from Bi 6s and O 2p hybrid orbitals to V 3d orbitals. The hybridization of the Bi 6s and O 2p levels makes the VB largely dispersed, which favors the mobility of photo-excitated holes and thus is beneficial to photocatalytic oxidation of organic pollutants [24].

The optical absorption property of a semiconductor, which is relevant to the electronic structure feature, is recognized as

Table 1
Size, band gap, BET surface areas and degradation rate of $BiVO_4$ samples

Samples	Average crystal size (nm)	Band gap (eV)	BET surface areas (m^2/g)	Degradation rate (%)
UR-$BiVO_4$	50	2.45	4.16	90
SSR-$BiVO_4$	200	2.30	0.26	8

the key factor in determining its photocatalytic activity [24,25]. The UV–vis diffuse reflectance spectra of UR- and SSR-$BiVO_4$ samples are shown in Fig. 3. The UR-$BiVO_4$ sample showed strong absorption in visible light region in addition to that in the UV light region. The steep shape of the spectrum indicated that the visible light adsorption is due to the band–gap transition [26], and the prolonged absorption tail until ~660 nm in the spectrum should result from the crystal defects formed at the instantly high temperature during ultrasound irradiation [10,22]. As a crystalline semiconductor, the optical absorption near the band edge follows the formula $\alpha h\nu = A(h\nu - E_g)^{n/2}$ [27], where α, ν, E_g and A are absorption coefficient, light frequency, band gap and a constant, respectively. Among them, n depends on the characteristics of the transition in a semiconductor, i.e. direct transition ($n=1$) or indirect transition ($n=4$). For $BiVO_4$, the value of n is 1. The energy of the band gap of $BiVO_4$ photocatalyst could be thus obtained from the plots of $(\alpha h\nu)^2$ versus photon energy ($h\nu$), as shown in inset of Fig. 3. The values estimated from the intercept of the tangents to the plots were 2.45 and 2.3 eV for UR-$BiVO_4$ and SSR-$BiVO_4$, respectively. The optical adsorption edge and the band gap of UR-$BiVO_4$ were blue-shifted in comparison with that of the SSR-$BiVO_4$, which was associated with the nanosized effect of UR-$BiVO_4$ crystals.

3.4. Photocatalytic activities

To study the photocatalytic activities of $BiVO_4$, methyl orange with a major absorption band at 464 nm was chosen as a model organic compound. As shown in Fig. 4, the absorption peaks of methyl orange solution gradually lower down during the photodegradation caused by UR-$BiVO_4$. The corresponding plot for the photodegradation rate of UR-$BiVO_4$ is shown in the inset of Fig. 4. The photodegradation rate is up to 90% in 30 min under visible light irradiation. As a comparison, the photodegradation rate of SSR-$BiVO_4$ (8%) was much lower. The phys-chemical properties of UR-$BiVO_4$ and SSR-$BiVO_4$ were compared and summarized in Table 1. The higher photocatalytic activities of UR-$BiVO_4$ can be ascribed to the small particle size and relatively large surface areas of UR-$BiVO_4$ as compared with that of SSR-$BiVO_4$. Generally, the activity of a photocatalyst increases with an increase in surface area not only because the photocatalytic reaction usually takes place on the catalyst surface but also the efficiency of the electron–hole separation is promoted [25,28]. On the other hand, both the photocatalytic degradation rate of UR-$BiVO_4$ and SSR-$BiVO_4$ were higher than that of standard product P25 (6%), which was reported to show high photocatalytic activity under UV-irradiation.

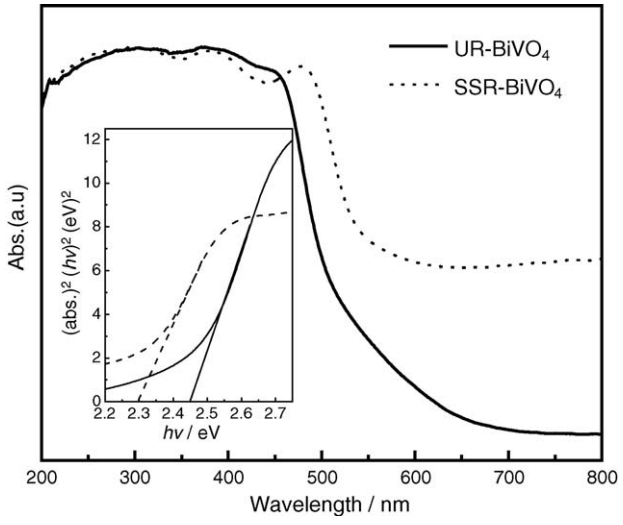

Fig. 3. UV–vis diffuse reflectance spectra of UR-$BiVO_4$ and SSR-$BiVO_4$ samples. Inset: plots of $(\alpha h\nu)^2$ vs. photon energy ($h\nu$).

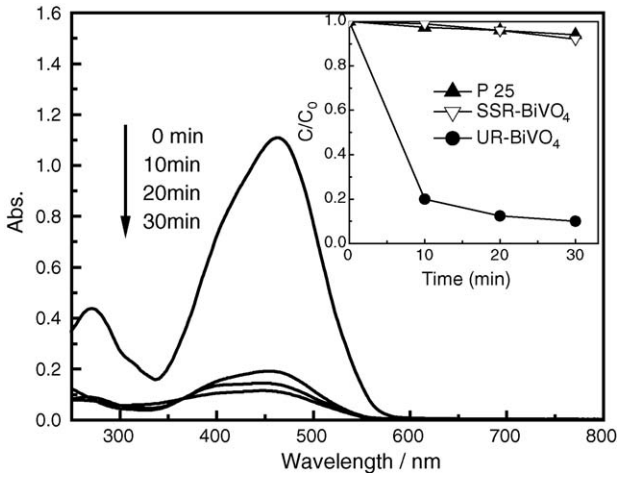

Fig. 4. Changes of UV–vis spectra of UR-$BiVO_4$ suspended MO solution as a function of irradiation time. Inset: MO concentration changes over UR-$BiVO_4$, SSR-$BiVO_4$ and P25, $\lambda > 400$ nm.

4. Conclusion

A facile sonochemical approach has been developed for the synthesis of visible-light-driven $BiVO_4$ photocatalyst. The average crystal size of as-prepared $BiVO_4$ particles is ca. 50 nm. Furthermore, the primary crystals that construct the as-prepared $BiVO_4$ particles share the same orientation along [1 1 0] direction. The as-prepared samples exhibited relatively high surface areas of ca. 4.16 m^2/g, which is about 16 times higher than that of the reference sample by solid-state reaction. The as-prepared $BiVO_4$ nanocrystals showed strong absorption in visible light region up to 660 nm in addition to that in the UV region. The band gap was estimated to be ca. 2.45 eV, representing an obvious

blue-shift compared with that of the bulk sample. The photodegradation rate of as-prepared $BiVO_4$ nanocrystals was quite high, up to 90% with 30 min visible light irradiation, which was much higher than that of the corresponding sample prepared by solid-state reaction (ca. 8%) and the standard photocatalyst P25 (ca. 6%) under the same conditions. The higher photocatalytic activities of as-prepared $BiVO_4$ nanocrystals are ascribed to the small particle size, higher BET surface areas and the unique electronic structure. This sonochemical route for the fabrication of $BiVO_4$ nanocrystal is effective, fast, convenient and environmentally friendly, and is thus worth to be extended to other photocatalysts systems.

Acknowledgements

We acknowledge the financial support from Chinese Academy of Sciences and Shanghai Institute of Ceramics under the program for Recruiting Outstanding Overseas Chinese (Hundred Talents Program).

References

[1] A. Fujishima, K. Honda, Nature 238 (1972) 37.
[2] Z. Zou, J. Ye, K. Sayama, H. Arakawa, Nature 414 (2001) 625.
[3] A. Fujishima, K. Hashimoto, T. Watanabe, TiO_2 Photocatalysis: Fundamentals and Applications, BKC, Inc., Tokyo, 1999.
[4] M.R. Hoffmann, S.T. Martin, W. Choi, D.W. Bahnemann, Chem. Rev. 95 (1995) 69.
[5] M. Yan, F. Chen, J. Zhang, M. Anpo, J. Phys. Chem. B 109 (2005) 8673.
[6] J.G. Yu, H.G. Yu, B. Cheng, X.J. Zhao, J.C. Yu, W.K. Ho, J. Phys. Chem. B 107 (2003) 13871.
[7] A. Kudo, K. Ueda, H. Kato, I. Mikami, Catal. Lett. 53 (1998) 229.
[8] S. Kohtani, M. Koshiko, A. Kudo, K. Tokumura, Y. Ishigaki, A. Toriba, K. Hayakawa, R. Nakagaki, Appl. Catal. B: Environ. 46 (2003) 573.
[9] S. Kohtani, J. Hiro, N. Yamamoto, A. Kudo, K. Tokumura, R. Nakagaki, Catal. Commun. 6 (2005) 185.
[10] A. Kudo, K. Omori, H. Kato, J. Am. Chem. Soc. 121 (1999) 11459.
[11] S. Tokunaga, H. Kato, A. Kudo, Chem. Mater. 13 (2001) 4624.
[12] A.R. Lim, S.H. Choh, M.S. Jang, J. Phys.: Condens. Matter. 7 (1995) 7309.
[13] A.K. Bhattacharya, K.K. Mallick, A. Hartridge, Mater. Lett. 30 (1997) 7.
[14] M. Gotić, S. Musić, M. Ivanda, M. Šoufek, S. Popović, J. Mol. Struct. 744–747 (2005) 535.
[15] A. Galembeck, O.L. Alves, Thin Solid Films 365 (2000) 90.
[16] M.M. Mdleleni, T. Hyeon, K.S. Suslick, J. Am. Chem. Soc. 120 (1998) 6189.
[17] N.A. Dhas, K.S. Suslick, J. Am. Chem. Soc. 127 (2005) 2368.
[18] T. Gao, Q. Li, T. Wang, Chem. Mater. 17 (2005) 887.
[19] J.G. Yu, M.H. Zhou, B. Cheng, H.G. Yu, X.J. Zhao, J. Mol. Catal. A 227 (2005) 75.
[20] K.S. Suslick, S.B. Choe, A.A. Cichowlas, M.W. Grinstaff, Nature 353 (1991) 414.
[21] H. Fu, C. Pan, W. Yao, Y. Zhu, J. Phys. Chem. B 109 (2005) 22432.
[22] D. Wang, J. Tang, Z. Zou, J. Ye, Chem. Mater. 17 (2005) 5177.
[23] M. Oshikiri, M. Boero, J. Ye, Z. Zou, G. Kido, J. Chem. Phys. 117 (2002) 7313.
[24] J. Tang, Z. Zou, J. Ye, Angew Chem. Int. Ed. 43 (2004) 4463.
[25] J. Tang, Z. Zou, J. Ye, Chem. Mater. 16 (2004) 1644.
[26] C. Zhang, Y. Zhu, Chem. Mater. 17 (2005) 3537.
[27] M.A. Butler, J. Appl. Phys. 48 (1977) 1914.
[28] J.G. Yu, J.F. Xiong, B. Cheng, S.W. Liu, Appl. Catal. B 60 (2005) 211.